

Revisiting the NVSS number count dipole

Prabhakar Tiwari^a and Adi Nusser^a

^aPhysics Department and the Asher Space Science Institute-Technion, Haifa 32000, Israel

E-mail: ptiwari@physics.technion.ac.il, adi@physics.technion.ac.il

Abstract. We present a realistic modeling of the NVSS number count dipole across the sky. The modeling relies on mock catalogues generated within the context of Λ CDM cosmology in the linear regime of structure formation. After removal of the solar motion dipole from the observation, the mocks show that the remaining signal is mostly (70%) due to contribution from large scale structure within $\sim 500\text{Mpc}$ ($z \sim 0.1$). The amplitude of this contribution depends on the bias factor of the NVSS galaxies. An effective bias factor $b(z < 0.1) < 2.0$ is ruled out at the $\sim 2.8\sigma$ significance by the comparison between the model and observed NVSS dipole. The mismatch is toned down to $\sim 2.3\sigma$ for $b(z) = 3$.

Keywords: Radio galaxies: high-redshift, Galaxies: active, Cosmology: large scale structure of the Universe,

Contents

1	Introduction	1
2	Data	2
3	Basics	3
3.1	Velocity Dipole	3
3.2	Angular Power Spectrum	3
3.3	The redshift distribution and galaxy biasing	4
4	The Mock catalogues	4
5	Results	5
6	Conclusion and Discussion	7
7	Acknowledgments	8

1 Introduction

The standard cosmological paradigm is based on “Cosmological Principle” [1, 2], i.e. the approach to homogeneity and isotropy of structure on the largest observable scales. Galaxies in the NRAO VLA Sky Survey (NVSS) [3] are typically assumed to lie at redshifts $z \sim 1$. At those high redshifts, the map of NVSS galaxy number count and flux density in the sky is expected to be nearly isotropic, after removal of the contribution of the local solar motion as measured by the Cosmic Microwave Background Radiation (CMBR) [4–9]¹. The solar motion results in an apparent dipole due to the Doppler and aberration effects [10]. The dipole signature is observed in number count as well as intensity maps generated from galaxies above a given flux density threshold. However, the dipole observation from NVSS is puzzling and several independent calculations for NVSS dipole [11–16] have found that the NVSS number dipole amplitude is inconsistent with the CMBR velocity dipole [12, 15, 16] at $\sim 3\sigma$ significance.

The first extraction of the solar motion from NVSS number count dipole was done by [11]. The authors [11] reported a velocity which was roughly in the same direction as CMBR but 1.5 to 2 times larger in amplitude. However, nine years later, using the same data a huge solar motion, $1600 \pm 400 \text{ km s}^{-1}$, was reported [12] from both the number count and brightness dipole measurements. This was in significant ($> 3\sigma$) disagreement with CMBR observations, which immediately attracted the attention of the community resulting in several detailed analyses of the NVSS dipole [13];[14]([17]);[15, 16].

The authors of [13] find a dipole almost six times larger than the CMBR prediction, however, the authors [13] attribute their deviation from CMBR prediction to observational bias. Another analysis by [14] yielded a dipole with an amplitude roughly three times larger than the prediction from the CMBR observed velocity dipole.

Finally, a recent analysis [15] of NVSS number dipole yielded the velocity values at $2.7 - 3.2\sigma$ deviation from the CMBR for various flux density cuts. Conclusively, the present status of NVSS dipole is a disagreement with CMBR predicted velocity dipole at 2.7σ or more. However, a detailed assessment of the contribution of the intrinsic variation of the number count as a result of the large scale structure remains to be done. This intrinsic dipole mainly depends on the following:

- number density distribution $N(z)$ as a function of redshift. This dictates the fractional contribution of the large scale structure from different redshifts.

¹The measured CMBR dipole magnitude is of order $\sim 10^{-3}$ [4–9] and the corresponding speed is found to be $369 \pm 0.9 \text{ km s}^{-1}$ in the direction, $l = 263.99^\circ \pm 0.14^\circ$, $b = 48.26 \pm 0.03^\circ$ in galactic coordinates [8, 9]. In J2000 equatorial coordinates, the direction parameters are $RA = 167.9^\circ$, $DEC = -6.93^\circ$.

- relation between the clustering of radio galaxies versus the underlying mass as a function of redshift. This biasing relation can be parametrized in terms of the galaxy and matter power spectrum as, $P_g(k, z) = b^2(z)P(k, z)$. The bias factor could be as large as $2 - 3$ and hence produce a significant enhancement to the dipole signal.
- constraints from the Local Universe. Our cosmological neighborhood within 100 Mpc is moving with $\sim 300 \text{ km s}^{-1}$ [18] and roughly aligned with the solar motion. This motion is caused by far large scale structures, producing an alignment between the solar motion and intrinsic dipole.

We aim at a realistic assessment of the NVSS dipole within the context of the Λ CDM model taking into account the above key ingredients. In Ref. [19] the authors use the best available redshift catalogs Combined EIS-NVSS Survey of Radio Sources (CENSORS)[20, 21] and Hercules [22, 23] and extract the biasing factor $b(z)$ as a function of redshift by matching the Λ CDM predictions to the NVSS measured power spectrum. The redshift dependent biasing [19] and number distribution are also found to be consistent with the observed radio luminosity functions [21, 24, 25]. The results obtained in [19] are based on the high order multipoles $l \geq 4$, where the analysis is fairly insensitive to complications related to the partial sky coverage. Here, we focus on the dipole and low multipoles $l \leq 4$. The contribution of the large scale structure to low multipoles is mainly due to low redshifts and about 70% (45%) of the dipole ($l = 4$) contribution comes from the redshift $z < 0.1$. Therefore, low multipoles essentially constrain the local galaxy biasing relation. The relatively large amplitude of the NVSS dipole requires a high bias factor at low redshifts ($z \lesssim 0.1$). We will show that the bias factor obtained from $l \geq 4$ [19], if extrapolated to $z \lesssim 0.1$ yields a $\sim 2.9\sigma$ disagreement between Λ CDM and the NVSS dipole. We will use different biasing templates to obtain the NVSS dipole prediction in mocks with an aim designed to match the NVSS data as much as possible.

The outline for the paper is as following. In Section 2, we give the data and observation details for NVSS. In Section 3.1 we review the velocity dipole formulation for a galaxy catalogue and in Section 3.2 we describe the formulation of the power spectrum for a partial sky. We give the number density $N(z)$ and biasing details in Section 3.3. All details and constraints used in mocks are described in Section 4. We present our results in Section 5 and finally in Section 6 we conclude and discuss our results.

2 Data

The NVSS observations are performed at 1.4GHz and the catalogue contains ~ 1.7 million sources at integrated flux density $S_{1.4\text{GHz}} > 2.5 \text{ mJy}$. The full width at half maximum resolution is 45 arcsec and nearly all observations are at uniform sensitivity. Most of the sources (90%) in catalogue are unresolved. The catalogue covers the sky north of declination -40° (J2000), which is almost 82% of the celestial sphere. However, the effective sky coverage for our studies is 75% as we mask the Galactic sources at latitudes $|b| < 5^\circ$ to avoid Galactic contamination and 22 sites around bright local extended radio galaxies identified by [11] to avoid overwhelming correlations at low scales. All the results in this paper follow these two cuts. Although, there are other relevant masks to avoid local contamination such as super Galactic plane and clustering dipole. The clustering dipole is masked by removing sources within 30 arcsec of known nearby galaxies as listed in [26–31]. The effect of these masks on dipole measurement in NVSS have been studied in detail by [15] and reported to affect the dipole within 10%. As in this paper we are interested in Λ CDM dipole, particular to NVSS galaxy catalogue, we ignore the clustering dipole and do not cross NVSS catalogue with any other catalogue to mask sources. Also, masking these catalogues may result as some artifact, if the masked galaxy catalogue is nonuniform over the NVSS observation area. Anyway these local catalogues masking does not affect the results more than 10% [15] and we safely ignore these masks.

In Ref. [11] it is shown that the NVSS has significant systematic gradient in surface density at flux densities $S < 15 \text{ mJy}$, which potentially affect the dipole and lower multipoles. Therefore, we restrict our analysis to sources brighter than 15 mJy. We consistently give the results for $S > 15, 20, 30, 40$ and 50 mJy . Furthermore, for completeness and comparison to other authors [11, 14, 15], we

give results for $S > 10$ mJy, for one set of mocks with most conservative parameters. We impose a maximum flux density cut $S < 1000$ mJy to remove extra bright sources.

3 Basics

3.1 Velocity Dipole

An observer moving with velocity \vec{v} sees the sky brighter in the forward direction due to Doppler boosting and aberration effects [10]. The flux density (energy per area per frequency) of sources in NVSS data follows a power-law dependence on frequency ν , $S \propto \nu^{-\alpha}$, with $\alpha \approx 0.75$ [10]. An intrinsic frequency ν_{rest} is measured by the moving observer at $\nu_{\text{obs}} = \nu_{\text{rest}}\delta$, where

$$\delta \approx 1 + (v/c) \cos \theta, \quad (3.1)$$

at the leading order. Therefore, the observed flux density is [10],

$$S_{\text{obs}} = S_{\text{rest}}\delta^{1+\alpha} \quad (3.2)$$

at a fixed frequency in observer's frame. The extragalactic radio source population count above some flux density cut, follows a power law $N(> S) \propto S^{-x}$ [10]. Therefore, the number count above some S_{obs} will change by a factor $\delta^{x(1+\alpha)}$ due to Doppler effect. In addition, the aberration of light changes the solid angle in the direction of motion,

$$d\Omega_{\text{obs}} = d\Omega_{\text{rest}}\delta^{-2}. \quad (3.3)$$

Using these two effects as in equation (3.2) and (3.3) the number count dipole due to the local motion, at leading order in v/c is given as [10, 15],

$$\vec{D} = [2 + x(1 + \alpha)](\vec{v}/c). \quad (3.4)$$

In above equation (3.4), the value of x can be obtained by a direct fit to the data. It has been observe that x slightly depends on lower flux density cut, S_{min} , indeed $x \sim 1$ [15].

3.2 Angular Power Spectrum

The comparison between mocks and NVSS observation is done via the angular power spectrum. Let $\mathcal{N}(\hat{\mathbf{r}})$ be the projected number density (per steradian) in the direction $\hat{\mathbf{r}}$, and $\bar{\mathcal{N}}$ be the mean number density averaged over the sky. We write the number density $\mathcal{N}(\hat{\mathbf{r}}) = \bar{\mathcal{N}}(1 + \Delta(\hat{\mathbf{r}}))$, where $\Delta(\hat{\mathbf{r}})$ represents the number surface density fluctuation of galaxies. We employ the HEALPix [32] equal area pixelization scheme to project galaxies in equal area pixels on a sphere. We expand the density contrast $\Delta(\hat{\mathbf{r}})$ in spherical harmonics, $Y_{lm}(\hat{\mathbf{r}})$, as

$$\Delta(\hat{\mathbf{r}}) = \sum_{l=1}^{\infty} \sum_{m=-l}^{+l} a_{lm} Y_{lm}(\hat{\mathbf{r}}). \quad (3.5)$$

For a full sky coverage, the harmonic coefficients, a_{lm} , can easily be calculated by inverting the equation (3.5), as

$$a_{lm} = \int_{4\pi} d\Omega \Delta(\hat{\mathbf{r}}) Y_{lm}(\hat{\mathbf{r}}). \quad (3.6)$$

The angular power, C_l , for multipole l is given as,

$$C_l = \langle |a_{lm}|^2 \rangle. \quad (3.7)$$

To account for the partial sky coverage of the NVSS observations, we resort to an approximate scheme [33] to compute C_l ,

$$C_l^{\text{obs}} = \frac{\langle |a'_{lm}|^2 \rangle}{J_{lm}} - \frac{1}{\bar{\mathcal{N}}} \quad (3.8)$$

where a'_{lm} is obtained from (3.6) but with angular integration over survey region only. Further, $J_{lm} = \int_{\text{survey}} |Y_{lm}|^2 d\Omega$ is the approximated correction suggested in reference [33]. The term $\frac{1}{N}$ describes the contribution of the Poissonian shot-noise. The C_l^{obs} is a measure of anisotropy at angular scale $\sim \pi/l$. The dipole term corresponds to C_1 and a precise relation to dipole amplitude, D ($|\vec{D}|$ from equation 3.4), is given as [13],

$$C_1 = \frac{4\pi}{9} D^2. \quad (3.9)$$

3.3 The redshift distribution and galaxy biasing

As in [19], we model the redshift distribution of NVSS galaxies relying on CENSORS [20, 21] and the Hercules [22, 23] surveys. The CENSORS catalogue was developed to study the evolution of the steep-spectrum radio luminosity function and the survey is presumably complete for flux densities $S > 7.2 \text{ mJy}$ at 1.4 GHz, containing 135 sources. Indeed, the catalogue covers only 6 deg^2 of the ESO Imaging Survey Patch D (EISD). The redshift measurements of the sample are 73% spectroscopically complete and for the remaining sources the redshift is estimated by Kz or Iz magnitude-redshift relation. The Hercules redshift survey of 64 sources within 1.2 deg^2 is complete for $S > 2 \text{ mJy}$ at 1.4 GHz. We use the combined CENSORS+Hercules data to model NVSS source redshift distribution. We find 133 sources above 10 mJy flux density S . For higher flux density cuts we use the same as the number of sources reduces significantly and effectively there is no change in fit. We emphasize that the CENSORS+Hercules combined data sets have been used to study the redshift dependent properties [19–21] and for NVSS data this is the best we can assume. We adopt the parametric form of $N(z)$, modeled in [19], as,

$$N^{\text{model}} \propto z^{a_1} \exp \left[- \left(\frac{z}{a_2} \right)^{a_3} \right]. \quad (3.10)$$

In [19] the free parameters, a_1 , a_2 and a_3 were fixed by fitting the CENSORS+Hercules redshift distribution as well as the NVSS angular power spectrum for $l > 4$. The best fit values were found to be $a_1 = 0.74 \pm 0.57$, $a_2 = 0.71 \pm 0.79$ and $a_3 = 1.06 \pm 0.53$.

A parametric fit for biasing $b(z) = 0.33z^2 + 0.85z + 1.6$, consistent with angular power spectrum for $l > 4$, is obtained in [19]. We adopt the same and explore possible dipole observation in mocks. Furthermore, we employ several other bias templates to fit with NVSS dipole observation.

The redshift number distribution from combined CENSORS+Hercules data sets is shown in figure (1). The redshift number distribution model fit (equation 3.10) and the outcomes from few mocks are also shown in same figure (1).

4 The Mock catalogues

We generate random Gaussian realization of the linear density field, δ_m , using **GRAFIC-2** [34]. The corresponding velocity field is computed using the linear theory relation between velocity and density [35]. We adopt the latest Planck results [36] for cosmological parameters: Hubble constant $H_0 = 67.8 \text{ km s}^{-1} \text{ Mpc}^{-1}$, total matter density parameter $\Omega_m = 0.308$, baryonic density parameter $\Omega_b = 0.0486$, linear clustering amplitude on $8h^{-1} \text{ Mpc}$ scale, $\sigma_8 = 0.815$ and a spectral index $n_s = 0.9667$. We use the fitting formulae from [37] for the ΛCDM power spectrum. The density and velocity fields are obtained in a periodic box of 512 grid points on the side. The comoving bin size is 34 Mpc, yielding a box comoving volume of $(34)^3 \times (512)^3 \text{ Mpc}^3$. This is equivalent to the comoving volume of the Universe out to redshift $z \sim 7$. “Observers” are placed at the centers of spheres of radius 100 Mpc having with bulk motions of $\sim 300 \text{ km s}^{-1}$. This is designed to match the observed bulk flow as measured in [18]. The biasing $b(z)$ and the linear growth factor $D(z)$ is followed from the modeling as in [19]. The mean number of the galaxies in a bin at redshift z_{bin} , $N(\text{bin})$, is,

$$N(\text{bin}) = \bar{n}(z_{\text{bin}}) \times dv \times [1 + b(z_{\text{bin}})D(z_{\text{bin}})\delta_m], \quad (4.1)$$

where $\bar{n}(z_{\text{bin}})$ is the mean number density at the bin and dv is the bin volume. The number density $\bar{n}(z_{\text{bin}})$ is obtained from the redshift distribution from the equation (3.10). The actual number of galaxies in the bin is a random integer, drawn from a Poisson distribution with mean $N(\text{bin})$.

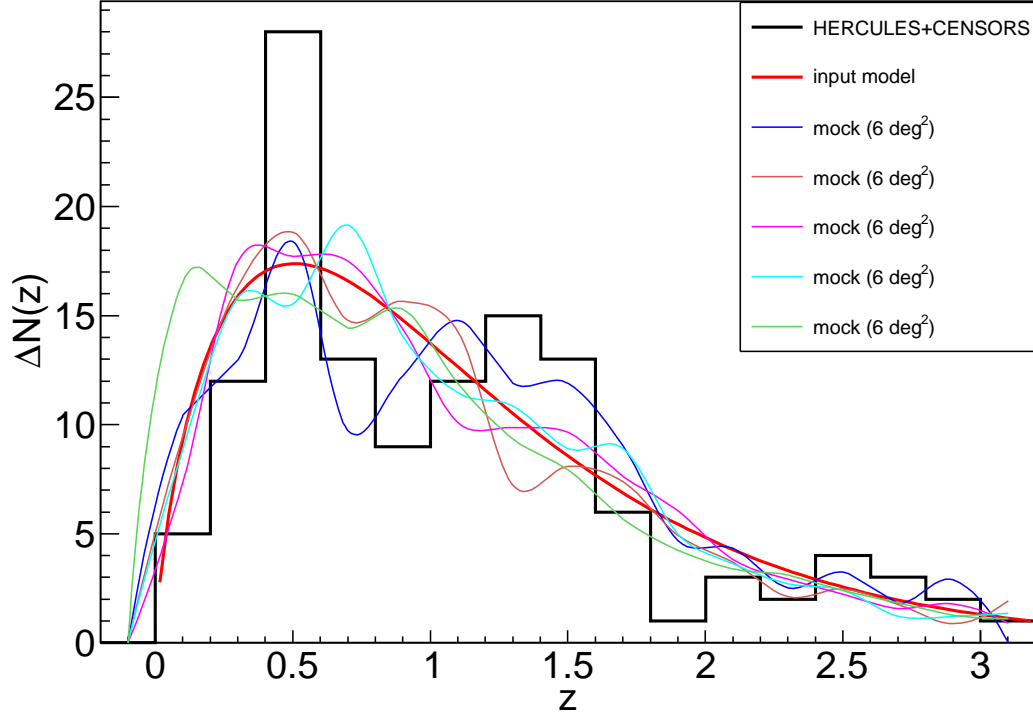


Figure 1. The histogram is the observed number of sources from combined CENSORS+Hercules data sets with flux density $S > 10$ mJy and per redshift bin $\Delta z = 0.2$. Best fit model (input model) follows equation (3.10) with parameters $a_1 = 0.74$, $a_2 = 0.71$ and $a_3 = 1.06$. The number density from mock catalogues for same area as observation is also shown. Note that the mocks include the Λ CDM density fluctuation, biasing $b(z)$ and the Poissonian shot-noise.

In order to include scatter due to uncertainties in the shape of $N(z)$, the mocks respectively correspond to a_1 , a_2 and a_3 , randomly drawn from their full probability distribution computed in [19]. Similarly, we also generate random realizations for bias $b(z)$. However, as the dipole (low multipoles) contribution is coming mostly from low redshifts data, hence insensitive to higher redshift $b(z)$ values. The data beyond redshift $z > 1.5$ have almost zero contribution to dipole as seen in figure (3). Therefore, the random outcomes of bias are terminated at redshift $z = 1.5$ and the bias is taken as $b(z > 1.5) = b(1.5)$. This is just to relax the computation. A comparison with best bias fit to random bias samples up to $z = 1.5$ is shown in figure (2).

The sky coverage of the data and direction of the observed dipole are also important inputs considered in mocks. We match these details exactly. We rotate the mocked map such as the dipole direction matches with the observed direction and then we mask the Galactic plane and 22 bright local extended sites as identified in [11]. We emphasize that the measured dipole amplitude depends on dipole direction and the mask location hence it is important to rotate the map to match with real data. Finally, this partial map, which closely resembles the NVSS map is used to calculate C_l . A good match in mocked C_l and the observation C_l is shown in figure (4).

5 Results

The statistical assessment of the ability of the models to match the observed C_1^{obs} is done by directly counting the number of mocks with C_1 exceeding the observed value. We perform this analysis for several lower cuts, S_{min} , on the flux density, S . For each flux cut, we generate 1,00,000 random mocks

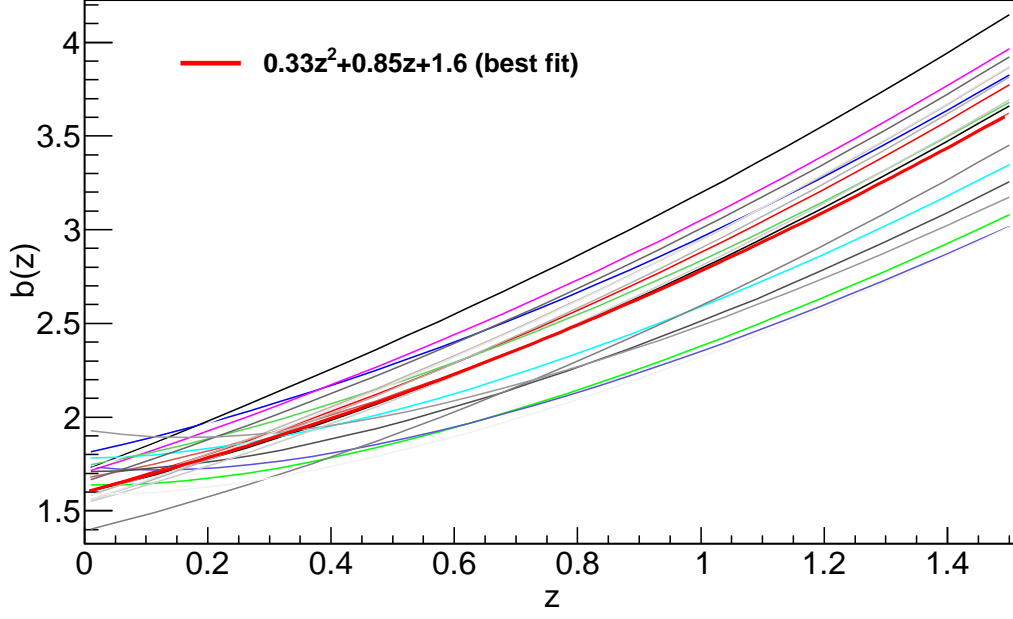


Figure 2. A few random outcomes of biasing factor $b(z)$ as a function of redshift, used in mocks. The polynomial fit as given in [19] is also shown as broad line.

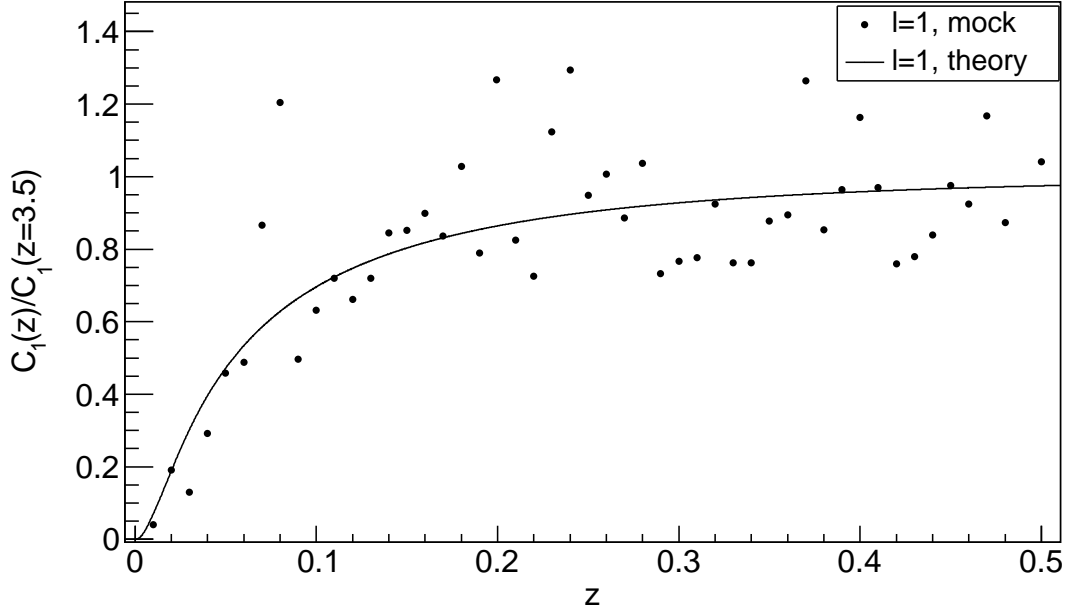


Figure 3. The mock $C_1(z)/C_1(z = 3.5)$ and the theoretical $C_1(z)/C_1(z = 3.5)$. The mock results are averaged over 100 density realizations and the normalization is done using the average $C_1(z)$ from redshift range $z = 0.3 - 0.5$.

and count the mocks with C_1 exceeding C_1^{obs} . The observed C_1^{obs} is calculated after removing the solar

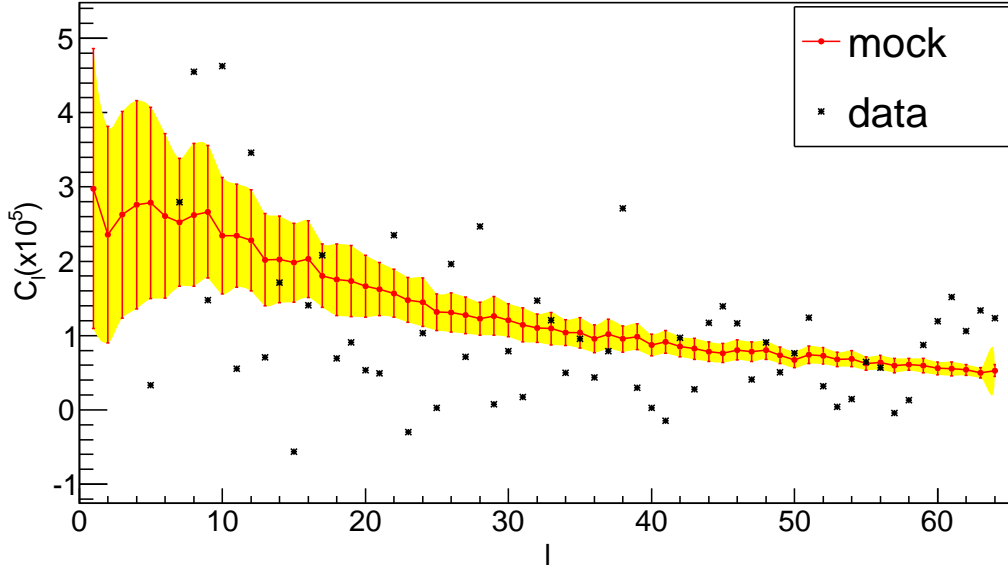


Figure 4. The mock C_l from 100 random samples and the observation C_l is shown for the flux density cut $S > 20$ mJy. This is for fix $b(z) = 3$, the mock’s dipole is closest to observation for this bias template.

motion contribution from NVSS number density maps. The mock’s C_1 distribution for $S_{\min} = 20$ mJy, with best fit biasing given in [19], is shown in figure 5. The C_1 distribution is the average of common variance of three independent Gaussian distribution ($\langle |a_{11}|^2 + |a_{10}|^2 + |a_{11}|^2 \rangle$), i.e. a χ^2 distribution with 3 degrees of freedom. A good fit to χ^2 distribution of 3 degrees of freedom is shown in figure 5. The NVSS observed and larger C_1 ($\geq 2.29 \times 10^{-4}$) outcomes are shown in green (dark) color. The probability for NVSS observed dipole (C_1^{obs}) is 0.2% including all possible kind of details. The probability 0.2% corresponds to $\sim 2.9\sigma$ significance level. Values of C_1^{obs} for several flux thresholds, S_{\min} , are summarised in Table 1. The results for $S > 10$ mJy have systematic biases [11], so not reliable, we only give $S > 10$ mJy results for completeness.

The dipole signal is mainly generated at low redshifts and hence constrains the low redshift bias. We denote $b'(z)$ as the bias input in mocks and $b(z)$ as the best fit bias from [19]. We use the bias templates $[b'(z < 0.1) = 2, b'(z \geq 0.1) = b(z)]$ and $[b'(z < 0.1) = 3, b'(z \geq 0.1) = b(z)]$ and find that the NVSS dipole observation excludes the effective bias $b(z) < 2$ in redshift range $z = 0 - 0.1$ at $\sim 2.8\sigma$ significance. The full results along with multipoles $l = 2, 3$ and 4 are shown in Table 3. We also consider an overall increase in bias $b(z)$, by using the template $[b'(z) = \frac{2.0 \times b(z)}{1.6}]$, the results are tabulated in Table 2. We find that the mocks with an effective bias $b(z)=3(\text{fix})$ give the largest dipole for different flux density cuts (Table 3) which is closest to the NVSS observed dipole. We verify that the fix bias $b(z)=3$ satisfies the observed C_l for all l ($l \leq 64$) (figure 4).

We include low multipoles $l = 2, 3$ and 4 along with dipole and give the results for different bias templates. The results are tabulated in Table 3.

6 Conclusion and Discussion

We have extended our previous work [19] on the angular clustering of NVSS sources to low multipole moments, focusing in particular on the dipole. These low multipoles are sensitive to the observational mask of the NVSS and require special treatment. Further, the NVSS number count may be affected by the presence of a large scale mass distribution which generates the observed bulk motion of a sphere of radius $100h^{-1}$ Mpc around the observer. The modeling here incorporates these effects as well as uncertainties in the redshift distribution, $N(z)$, of the NVSS sources. The form of $N(z)$ and

S_{\min} (mJy)	(RA, Dec)	(l, b)	C_1 ($\times 10^4$)	shot-noise ($\times 10^5$)	p-value	σ - significance
10	(135°, 23°)	(204°, 38°)	1.00	1.8	0.02389	1.98
15	(151°, -6°)	(246°, 38°)	1.35	2.5	0.01696	2.12
20	(151°, -14°)	(253°, 32°)	2.29	3.3	0.00193	2.89
30	(160°, -16°)	(263°, 36°)	2.84	4.7	0.00262	2.79
40	(150°, -35°)	(268°, 16°)	3.52	6.3	0.00173	2.92
50	(174°, -36°)	(286°, 24°)	4.59	8.0	0.00209	2.86

Table 1. The observed C_1^{obs} (including shot-noise) and shot-noise ($\frac{1}{N}$) along with dipole direction. The dipole direction is the vector average over data region whereas the mask data region have given the average weight. The probability is the count of mocks with C_1 increasing observation C_1^{obs} . The corresponding σ - significance is also given for the observed probability. The counting is done for 1,00,000 samples. We have done sampling over best biasing fit $b(z) = 0.33z^2 + 0.85z + 1.6$ and $N(z)$. The p-value is the probability ($C_1 > C_1^{\text{obs}}$).

S_{\min} (mJy)	15	20	30	40	50
Probability ($C_1 > C_1^{\text{obs}}$)	0.03871	0.00512	0.00563	0.00387	0.00300
σ - significance	1.77	2.57	2.53	2.66	2.75

Table 2. The probability and significance of C_1^{obs} if we scale the bias slightly. The bias used in mocks is $b'(z)$. The $b'(z)$ to best fit bias $b(z)$ relation is $b'(z) = \frac{2.0 \times b(z)}{1.6}$. Note the factor $\frac{2.0}{1.6}$, this is just ad-hoc to have $b'(z=0) = 2$. We have done sampling over best biasing fit $b(z)$ and $N(z)$.

the bias factor $b(z)$ are randomly drawn from the full probability distribution given in [19]. The velocity constraint helps to obtain a large dipole to match the observation. The effect of velocity constraint, as compared to random velocity bins as observer bins, is given in Table 4. The rotation of mock map to match with observed dipole direction also helps in yielding a slightly higher dipole. However, the main effect is related to the bias b of radio galaxies. The NVSS observed dipole and quadrupole are mostly shaped at low redshifts $z \lesssim 0.1$. Thus these multipoles probe ~ 500 Mpc scales rather than ultra large distances of few Gpc ($z \sim 1$). The dipole and quadrupole require a larger bias factor than the value obtained by [19] for the higher order C_l . Increasing the bias ($b \sim 3$) at low redshifts ($z \lesssim 0.1$) tones down the NVSS dipole to a $\sim 2.3\sigma$ significance (for $S > 20, 30, 40$ and 50 mJy). For the dipole of $S > 20$ mJy sources, we get $b(z) \geq 2.0$ at $\sim 2.8\sigma$. This result is consistent with the constraint $b\sigma_8 < 1.87$ obtained in [38]. However, we emphasize that these authors exclude the dipole in the derivation of this constraint. The bias templates used in our work are comparable with most of the bias values in literature. The [39] and [40] deduced bias values agrees well with all our bias templates. However, the bias in [41] shows some disagreement with our bias values at low redshifts.

The relatively high amplitude of NVSS dipole can be largely explained in terms of the radio galaxy biasing at low redshifts. It could also be due to a residual calibration error across the sky, but this should not affect the high flux thresholds that have been considered in NVSS dipole calculations. Further, presence of a large local void as suggested by [42] could significantly contribute to number count dipole and partially explain the NVSS excess dipole. Although, the authors [42] conclude that a single realistic void can not explain the excess NVSS dipole completely.

7 Acknowledgments

This research was supported by the I-CORE Program of the Planning and Budgeting Committee, THE ISRAEL SCIENCE FOUNDATION (grants No. 1829/12 and No. 203/09), the Asher Space

S_{\min} (mJy)	C_1		C_2		C_3		C_4	
	p-value	σ -significance	p-value	σ -significance	p-value	σ -significance	p-value	σ -significance
$b'(z < 0.1) = 2$ and $b'(z \geq 0.1) = b(z)$								
15	0.01314	2.22	0.00235	2.83	0.31450	0.48	0.11169	1.22
20	0.00149	2.97	0.00448	2.61	0.96804	-1.85	0.03179	1.86
30	0.00258	2.80	0.00738	2.44	0.68488	-0.48	0.29305	0.54
40	0.00233	2.83	0.00672	2.47	0.40229	0.25	0.40216	0.25
50	0.00133	3.00	0.08371	1.38	0.46301	0.09	0.30358	0.51
$b'(z) = 2.0$								
15	0.01437	2.19	0.00324	2.72	0.32412	0.46	0.12362	1.16
20	0.00149	2.97	0.00493	2.58	0.96881	-1.86	0.03533	1.81
30	0.00300	2.75	0.00765	2.43	0.69182	-0.50	0.30641	0.51
40	0.00252	2.80	0.00696	2.46	0.41254	0.22	0.41076	0.23
50	0.00154	2.96	0.08581	1.37	0.46751	0.08	0.31316	0.49
$b'(z < 0.1) = 3$ and $b'(z \geq 0.1) = b(z)$								
15	0.03509	1.81	0.00771	2.42	0.40814	0.23	0.17602	0.93
20	0.00427	2.63	0.01006	2.32	0.97681	-1.99	0.05376	1.61
30	0.00547	2.55	0.01409	2.20	0.73469	-0.63	0.35006	0.39
40	0.00485	2.59	0.01058	2.31	0.44734	0.13	0.44691	0.13
50	0.00263	2.79	0.10905	1.23	0.50088	-0.00	0.33613	0.42
$b'(z) = 3.0$								
15	0.06170	1.54	0.02345	1.99	0.56519	-0.16	0.34328	0.40
20	0.00922	2.36	0.02290	2.00	0.98633	-2.21	0.13678	1.10
30	0.01011	2.32	0.02437	1.97	0.80103	-0.85	0.49466	0.01
40	0.00656	2.48	0.01882	2.08	0.53594	-0.09	0.56074	-0.15
50	0.00391	2.66	0.13536	1.10	0.57366	-0.19	0.43821	0.16

Table 3. The low multipole C_1 , C_2 , C_3 and C_4 for different biasing templates. The negative significance indicate that the mock's values are above observation. The p-value is the probability ($C_l > C_l^{\text{obs}}$)

S_{\min} (mJy)	15	20	30
considering all constraints			
Probability ($C_1 > C_1^{\text{obs}}$)	0.01696	0.00193	0.00262
σ -significance	2.12	2.88	2.79
No velocity constraint			
Probability ($C_1 > C_1^{\text{obs}}$)	0.01625	0.00175	0.00224
σ -significance	2.14	2.92	2.84
No rotation to map			
Probability ($C_1 > C_1^{\text{obs}}$)	0.01280	0.00136	0.00238
σ -significance	2.23	3.00	2.82

Table 4. The dependence of C_1 to different constraints used in mocks. The results are show for flux density cut $S > 15, 20$ and 30 mJy.

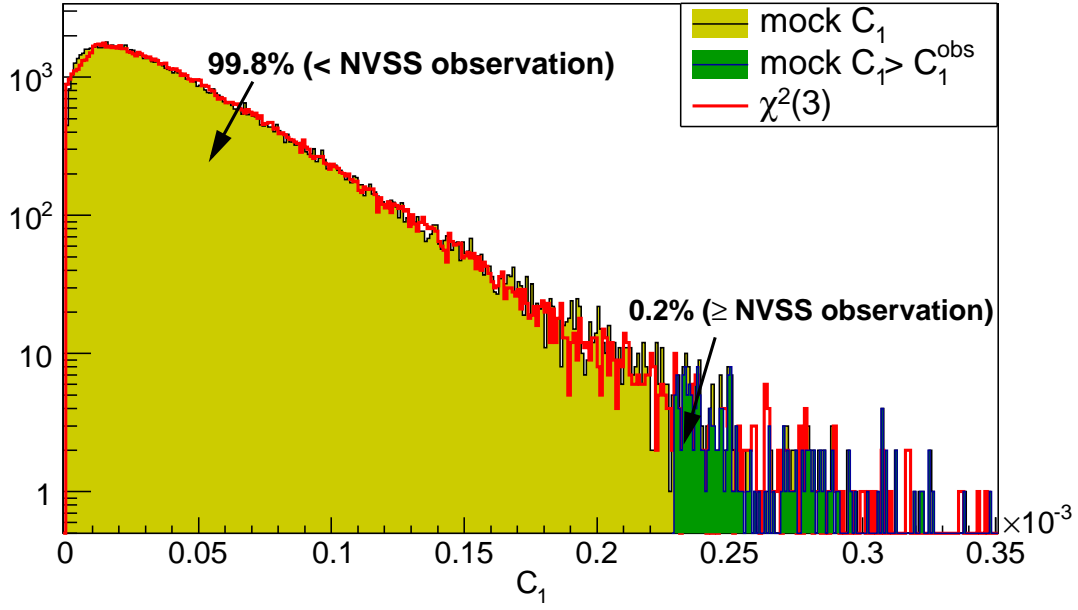


Figure 5. The mocks C_1 distribution and the observation probability from 1,00,000 samples is shown for the flux density cut $S > 20$ mJy. Note that the y-axis is in log scale as the probability for NVSS observed dipole or a dipole with larger amplitude is extremely tiny (0.2%) and not even visible in linear scale. A good fit to mocks C_1 distribution to $\chi^2(3)$ probability distribution is also shown.

Research Institute, and the Munich Institute for Astro and Particle Physics (MIAPP) of the DFG cluster of excellence Origin and Structure of the Universe. We have used CERN ROOT 5.34/21 [43] for generating our plots.

References

- [1] E. A. Milne, *World-Structure and the Expansion of the Universe*, *Zeitschrift für Astrophysik* **6** (1933) 1.
- [2] E. A. Milne, *Relativity, gravitation and world-structure*. 1935.
- [3] J. J. Condon, W. D. Cotton, E. W. Greisen, Q. F. Yin, R. A. Perley, G. B. Taylor, and J. J. Broderick, *The NRAO VLA Sky Survey*, *AJ* **115** (May, 1998) 1693–1716.
- [4] E. K. Conklin, *Velocity of the Earth with Respect to the Cosmic Background Radiation*, *Nature* **222** (June, 1969) 971–972.
- [5] P. S. Henry, *Isotropy of the 3 K Background*, *Nature* **231** (June, 1971) 516–518.
- [6] B. E. Corey and D. T. Wilkinson, *A Measurement of the Cosmic Microwave Background Anisotropy at 19 GHz*, in *Bulletin of the American Astronomical Society*, vol. 8 of *Bulletin of the American Astronomical Society*, p. 351, Mar., 1976.
- [7] G. F. Smoot, M. V. Gorenstein, and R. A. Muller, *Detection of anisotropy in the cosmic blackbody radiation*, *Physical Review Letters* **39** (Oct., 1977) 898–901.
- [8] A. Kogut, C. Lineweaver, G. F. Smoot, C. L. Bennett, A. Banday, et al., *Dipole anisotropy in the COBE differential microwave radiometers first-year sky maps*, *ApJ* **419** (1993) 1, [[astro-ph/9312056](#)].
- [9] G. Hinshaw, J. L. Weiland, R. S. Hill, N. Odegard, C. Larson, et al., *Five-Year Wilkinson Microwave Anisotropy Probe Observations: Data Processing, Sky Maps, and Basic Results*, *ApJS* **180** (2009) 225, [[arXiv:0803.0732](#)].

- [10] G. F. R. Ellis and J. E. Baldwin, *On the expected anisotropy of radio source counts*, *MNRAS* **206** (Jan., 1984) 377–381.
- [11] C. Blake and J. Wall, *Detection of the velocity dipole in the radio galaxies of the nrao vla sky survey*, *Nature* **416** (2002) 150–152, [[astro-ph/0203385](#)].
- [12] A. K. Singal, *Large Peculiar Motion of the Solar System from the Dipole Anisotropy in Sky Brightness due to Distant Radio Sources*, *ApJL* **742** (Dec., 2011) L23, [[arXiv:1110.6260](#)].
- [13] C. Gibelyou and D. Huterer, *Dipoles in the Sky*, *MNRAS* **427** (2012) 1994–2021, [[arXiv:1205.6476](#)].
- [14] M. Rubart and D. J. Schwarz, *Cosmic radio dipole from nvss and wenss*, *A&A* **555** (2013), no. A117 [[arXiv:1301.5559](#)].
- [15] P. Tiwari, R. Kothari, A. Naskar, S. Nadkarni-Ghosh, and P. Jain, *Dipole anisotropy in sky brightness and source count distribution in radio NVSS data*, *Astroparticle Physics* **61** (Feb., 2015) 1–11, [[arXiv:1307.1947](#)].
- [16] P. Tiwari and P. Jain, *Dipole anisotropy in integrated linearly polarized flux density in NVSS data*, *MNRAS* **447** (Mar., 2015) 2658–2670, [[arXiv:1308.3970](#)].
- [17] A. K. Singal, *Comment on "Cosmic radio dipole from NVSS and WENSS"*, *Astron.Astrophys.* **568** (2014) A63, [[arXiv:1408.0679](#)].
- [18] A. Nusser and M. Davis, *The cosmological bulk flow: consistency with Λ CDM and $z \approx 0$ constraints on σ_8 and γ* , *Astrophys.J.* **736** (2011) 93, [[arXiv:1101.1650](#)].
- [19] A. Nusser and P. Tiwari, *The Clustering of Radio Galaxies: Biasing and Evolution Versus Stellar Mass*, *ApJ* **accepted** (2015) [[arXiv:1505.06817](#)].
- [20] P. N. Best, J. N. Arts, H. J. A. Röttgering, R. Rengelink, M. H. Brookes, and J. Wall, *CENSORS: A Combined EIS-NVSS Survey Of Radio Sources - I. Sample definition, radio data and optical identifications*, *MNRAS* **346** (Dec., 2003) 627–683, [[astro-ph/0308401](#)].
- [21] E. E. Rigby, P. N. Best, M. H. Brookes, J. a. Peacock, J. S. Dunlop, H. J. a. Röttgering, J. V. Wall, and L. Ker, *The luminosity-dependent high-redshift turnover in the steep spectrum radio luminosity function: Clear evidence for downsizing in the radio-AGN population*, *Monthly Notices of the Royal Astronomical Society* **416** (2011), no. 3 1900–1915, [[arXiv:1104.5020](#)].
- [22] I. Waddington, R. A. Windhorst, J. S. Dunlop, D. C. Koo, and J. A. Peacock, *The LBDS Hercules sample of mJy radio sources at 1.4GHz - I. Multicolour photometry*, *MNRAS* **317** (Oct., 2000) 801–824, [[astro-ph/0006169](#)].
- [23] I. Waddington, J. S. Dunlop, J. A. Peacock, and R. A. Windhorst, *The LBDS Hercules sample of mJy radio sources at 1.4 GHz - II. Redshift distribution, radio luminosity function, and the high-redshift cut-off*, *MNRAS* **328** (Dec., 2001) 882–896, [[astro-ph/0107048](#)].
- [24] T. Mauch and E. M. Sadler, *Radio sources in the 6dFGS: local luminosity functions at 1.4 GHz for star-forming galaxies and radio-loud AGN*, *Monthly Notices of the Royal Astronomical Society* **375** (Mar., 2007) 931–950, [[0612018](#)].
- [25] V. Smolcic, E. Schinnerer, G. Zamorani, E. F. Bell, M. Bondi, C. L. Carilli, P. Ciliegi, B. Mobasher, T. Paglione, M. Scodeggio, and N. Scoville, *The dust un-biased cosmic star formation history from the 20 cm VLA-COSMOS survey*, *The Astrophysical Journal* **13** (2008), no. 77 9, [[arXiv:0808.0493](#)].
- [26] G. de Vaucouleurs, A. de Vaucouleurs, H. G. Corwin, R. J. Buta, G. Paturel, and P. Fouque, *Third Reference Catalogue of Bright Galaxies (RC3)*. Springer-Verlag, New York, 1991.
- [27] H. Corwin, Jr., R. Buta, and G. de Vaucouleurs, *Corrections and additions to the third reference catalogue of bright galaxies*, *AJ* **108** (Dec., 1994) 2128–2144.
- [28] W. Saunders, W. Sutherland, S. Maddox, O. Keeble, S. Oliver, et al., *The PSCz catalogue*, *MNRAS* **317** (2000) 55, [[astro-ph/0001117](#)].
- [29] T. H. Jarrett, T. Chester, R. Cutri, S. E. Schneider, and J. P. Huchra, *The 2MASS Large Galaxy Atlas*, *AJ* **125** (Feb., 2003) 525–554.
- [30] J. P. Huchra, L. M. Macri, K. L. Masters, T. H. Jarrett, P. Berlind, et al., *The 2mass redshift survey-description and data release*, *ApJS* **199** (Apr., 2012) 26, [[arXiv:1108.0669](#)].

- [31] M. Bilicki, T. H. Jarrett, J. A. Peacock, M. E. Cluver, and L. Steward, *Two micron all sky survey photometric redshift catalog: A comprehensive three-dimensional census of the whole sky*, *The Astrophysical Journal Supplement Series* **210** (2014), no. 1 9.
- [32] K. Gofski, E. Hivon, A. Banday, B. Wandelt, F. Hansen, et al., *Healpix - a framework for high resolution discretization, and fast analysis of data distributed on the sphere*, *ApJ* **622** (2005) 759–771, [[astro-ph/0409513](#)].
- [33] P. J. E. Peebles, *The large-scale structure of the universe*. Princeton University Press, 1980.
- [34] E. Bertschinger, *Multiscale Gaussian random fields for cosmological simulations*, *Astrophys.J.Suppl.* **137** (2001) 1, [[astro-ph/0103301](#)].
- [35] P. J. E. Peebles, *The large-scale structure of the universe*. 1980.
- [36] Planck Collaboration, R. Adam, P. A. R. Ade, N. Aghanim, Y. Akrami, M. I. R. Alves, M. Arnaud, F. Arroja, J. Aumont, C. Baccigalupi, and et al., *Planck 2015 results. I. Overview of products and scientific results*, *ArXiv e-prints* (Feb., 2015) [[arXiv:1502.01582](#)].
- [37] D. J. Eisenstein and W. Hu, *Baryonic Features in the Matter Transfer Function*, *ApJ* **496** (Mar., 1998) 605–614, [[astro-ph/9709112](#)].
- [38] C. Blake, P. G. Ferreira, and J. Borrill, *The angular power spectrum of NVSS radio galaxies*, *MNRAS* **351** (July, 2004) 923–934, [[astro-ph/0404085](#)].
- [39] R. Allison, S. N. Lindsay, B. D. Sherwin, F. de Bernardis, J. R. Bond, E. Calabrese, M. J. Devlin, J. Dunkley, P. Gallardo, S. Henderson, A. D. Hincks, R. Hlozek, M. Jarvis, A. Kosowsky, T. Louis, M. Madhavacheril, J. McMahon, K. Moodley, S. Naess, L. Newburgh, M. D. Niemack, L. A. Page, B. Partridge, N. Sehgal, D. N. Spergel, S. T. Staggs, A. van Engelen, and E. J. Wollack, *The Atacama Cosmology Telescope: measuring radio galaxy bias through cross-correlation with lensing*, *MNRAS* **451** (July, 2015) 5368–5377, [[arXiv:1502.06456](#)].
- [40] S. N. Lindsay, M. J. Jarvis, M. G. Santos, M. J. I. Brown, S. M. Croom, S. P. Driver, A. M. Hopkins, J. Liske, J. Loveday, P. Norberg, and A. S. G. Robotham, *Galaxy and Mass Assembly: the evolution of bias in the radio source population to $z \sim 1.5$* , *MNRAS* **440** (May, 2014) 1527–1541, [[arXiv:1402.5654](#)].
- [41] S. N. Lindsay, M. J. Jarvis, and K. McAlpine, *Evolution in the bias of faint radio sources to $z \sim 2.2$* , *MNRAS* **440** (May, 2014) 2322–2332, [[arXiv:1403.0882](#)].
- [42] M. Rubart, D. Bacon, and D. J. Schwarz, *Impact of local structure on the cosmic radio dipole*, *A&A* **565** (May, 2014) A111, [[arXiv:1402.0376](#)].
- [43] R. Brun, F. Rademakers, et al., *ROOT web page*, <http://root.cern.ch/>, 2001.